

# Evaluation of 3C-SiC Nanomechanical Resonators Using Room Temperature Magnetomotive Transduction

Seong Chan Jun, X. M. Henry Huang, and J. Hone  
Mechanical Engineering and NSEC  
Columbia University  
New York, NY, USA  
scj10@columbia.edu

C. A. Zorman, and M. Mehregany  
Department of Electrical Engineering & Computer Science  
Case Western Reserve University  
Cleveland, OH, USA  
caz@case.edu

**Abstract**— We report our efforts toward using room temperature magnetomotive transduction technique for SiC nanomechanical resonators. The resonators were nanomachined from 30 nm-thick 3C-SiC thin films epitaxially grown on (100) silicon. The structures show mechanical resonance at 10.41 MHz with a quality factor of about 2800. Magnetomotive transduction was used to read out the resonance at room temperature and moderate pressure. This technique has the potential to become an important tool for studying the properties of ultrathin films, as well as developing deployable SiC-based NEMS prototype devices and systems for applications that would benefit from SiC as the structural material.

## I. INTRODUCTION

Nanoelectromechanical systems (NEMS) have offered great promise for applications in mechanical signal processing and ultrasensitive detection [1-4]. As device dimensions are reduced, the frequency of NEMS devices can reach the MHz to GHz regime. At the same time, the small size of the devices ensures low operating power, high responsivity, and parameter tunability. A number of methods, including magnetomotive transduction, optical interferometry, and capacitive detection, have been used to detect device motion, but readout in general represents a primary challenge in the NEMS field.

SiC has emerged as a versatile structure material for nanoelectromechanical systems (NEMS) devices. Its high Young's modulus-to-density ratio has proven advantageous for improving the performance of ultrahigh and microwave frequency nanomechanical resonators [5], which in turn are demonstrated to be useful for a number of important research directions, including nanomechanical mass detection [6], mechanical parametric amplification [7] and quantum measurement device prototyping [8]. In the examples cited above, a magnetomotive transduction technique was used to excite the resonators and measure their response. The

required high magnetic field was provided by a superconducting magnet in a cryostat under extremely low temperature conditions. Such an approach provides excellent experimental performance, but presents a significant obstacle to implementing these devices in many applications. Ideally, this scheme could be used at room temperature and as close as possible to atmospheric pressure. In addition, low-cost and portable components are essential for applications. In this paper, we report efforts toward using magnetomotive transduction at room temperature and moderate vacuum. This approach is applied to SiC resonators. The demonstration of 'table-top' NEMS operation points toward practical implementation of NEMS devices in a variety of real-world settings.

## II. NANOMECHANICAL RESONATOR

Ultrathin single crystal 3C-SiC films are grown on a silicon wafer by a heteroepitaxial APCVD process [9]. SiH<sub>4</sub> and C<sub>3</sub>H<sub>8</sub> are used as precursors, and H<sub>2</sub> is used as a carrier gas. The epitaxial process is a two-step, high-temperature (1280°C) procedure, involving the carbonization of the Si surface in a C<sub>3</sub>H<sub>8</sub>/H<sub>2</sub> ambient followed by epitaxial growth using SiH<sub>4</sub>, C<sub>3</sub>H<sub>8</sub>, and H<sub>2</sub>. The films used in this study were 30 nm in thickness. The surface roughness of these films was found to be well below 1 nm.

The nanoscale resonators were fabricated using electron-beam lithography combined with reactive ion etching. Standard PMMA resist (495 KDa, 4% in anisole) is spun onto diced chip, then baked at 180°C. The device pattern is defined by electron beam lithography. After development in MIBK:IPA (1:3) solution, a 30nm thick aluminum layer is thermally evaporated onto the chip. Liftoff in acetone is then performed to remove aluminum in areas covered by PMMA after resist development, thus transferring the desired device pattern to the metallic layer on top of SiC surface. An RIE process with CF<sub>4</sub>/O<sub>2</sub> (9 to 1 ratio) gas mixture is used to etch the SiC layer anisotropically. The RF power is 100 W at a

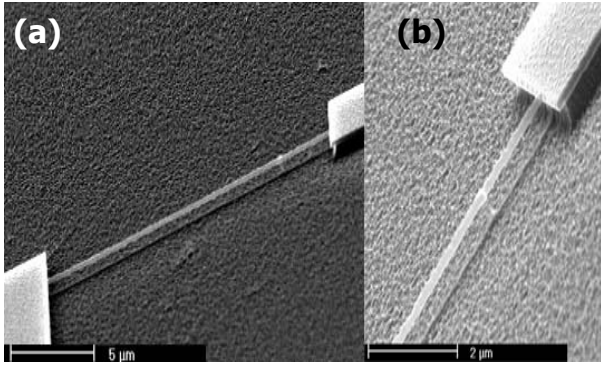


Figure 1. SEM image of the device under test (a) 12 μm long and 100nm wide 30nm thick SiC, capped with a 30 nm Al layer, and (b) magnified view of the clamping region.

gas pressure 250 mTorr. After a total of 2 minutes of etching, this recipe first clears the silicon carbide film not covered by aluminum, then etches into the silicon substrate isotropically, thereby releasing the doubly-clamped beam device structure. The aluminum layer serves as both etch mask and conductive layer for later device testing. The etch rate for aluminum is found to be negligible. Because the SiC etch is highly anisotropic, the device layer is preserved intact as the supporting Si is isotropically etched to provide the undercut structure. An SEM image of a completed pair of devices is shown in Figure 1a, with a zoom-in view showing the

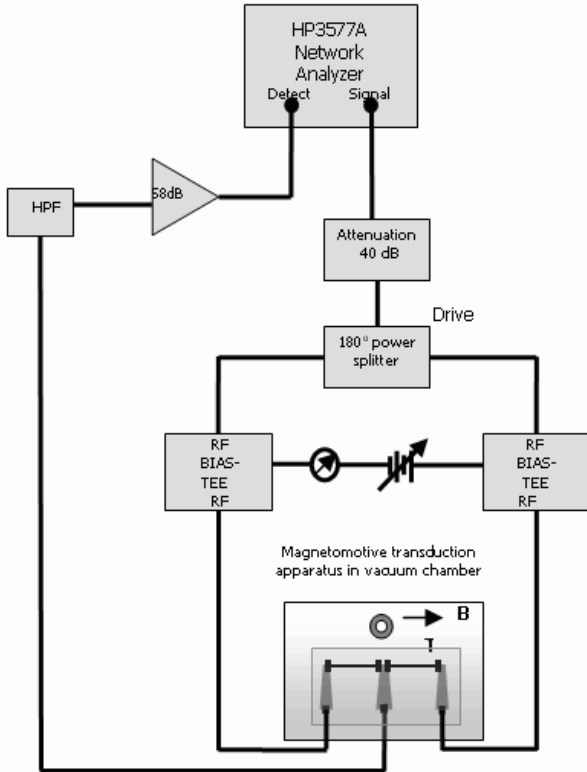


Figure 2. Schematic circuit diagram used for mechanical resonance measurement

suspension of the nanostructure in Figure 1b. The geometry of the resonator beams are: 12μm long, 100 nm wide, 30nm Al on top of 30nm SiC.

### III. PRINCIPLES OF BEAM MOTION

The dynamic behavior of a flexural beam with zero tension case is most easily treated using the Euler-Bernoulli theory [10], for isotropic material, the transverse displacement  $Y(x,t)$  of beam center line along the  $y$  direction, obeys the differential equation

$$\rho A \frac{\partial^2 Y}{\partial t^2}(x,t) = - \frac{\partial^2}{\partial x^2} EI \frac{\partial^2 Y}{\partial x^2}(x,t) \quad (1)$$

where  $\rho$  is the material density,  $A=wt$  is the cross-sectional area,  $E$  is Young's modulus, and  $I=wt^3/12$  is the bending moment of inertia. The clamped ends, at  $x=0$  and  $x=L$ , impose the boundary conditions  $Y(0)=Y(L)=0$  and  $Y'(0)=Y'(L)=0$ . The solutions have the form

$$Y_n(x,t) = (C_{1n}(\cos k_n x - \cosh k_n x) + C_{2n}(\sin k_n x - \sinh k_n x)) \exp(i\Omega_n t) \quad (2)$$

with eigenvectors  $k_n$  satisfying  $\cos k_n L \cosh k_n L = 1$ .

In this resonator, magnetomotive transduction is used for device testing [11-13]. Simply put, it detects the EMF voltage as the resonant motion cuts the magnetic field lines. The motion is induced by sending an RF current through the beam, which applies an alternating force at that frequency due to the presence of the B field. The frequency of the RF current, thus the frequency of the applied force, is swept nearby the estimated fundamental flexural mode resonance frequency. When the drive frequency is off from the mechanical resonance, the induced motion is minimal, thus essentially no additional EMF is generated; at resonance, the motion is significantly enhanced, and a peak in the EMF is seen. Because both the drive amplitude and induced EMF are proportional to magnetic field, the peak height varies as  $B^2$ , justifying the use of superconducting magnets for high fields. However, a smaller field, produced by a permanent magnet, can be used if the length of the beam is increased to offset the reduction in magnetic field.

### IV. DEVICE OPERATION

To optimize the electrical readout the circuit diagram is designed as Figure 2. The RF drive and readout is accomplished with a network analyzer (HP 3577A). Two resonators are fabricated side-by-side to form an RF resistance bridge. The two arms of the bridge are driven out of phase by passing the drive signal through a 180° power splitter. In this way, the middle arm of the device is at virtual ground, and the background of is significantly reduced.

In this work, we have constructed a room-temperature table-top apparatus as shown in Figure 3. That is capable of performing magnetomotive testing on nanomechanical

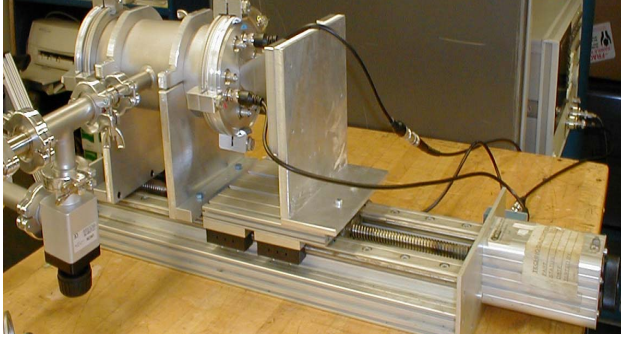


Figure 3. Photograph of the magnetomotive transduction apparatus for nanomechanical testing at room temperature, showing a turbo-pumped vacuum chamber, the NdFeB permanent magnet and test equipment used.

resonators without the need for cryogenic temperatures and superconducting magnets. The operation of this setup has been previously demonstrated [14, 15] for AuPd alloy nanomechanical resonators.

The device is wire bonded and loaded into a vacuum chamber that is evacuated by a small dry mechanical pump capable of achieving pressures of  $\sim 1$  Torr, which are sufficient for high-Q operation of the NEMS resonators. Electrical feedthroughs allow connections between the devices and test equipment. An NdFeB permanent magnet is mounted nearby the device and used for magnetomotive detection of mechanical resonance. The magnet provides a field up to 0.9 T at the test chip. The field is variable by mechanically shifting the position of the magnet relative to the sample. The magnet is oriented properly so that the field lines are perpendicular to the sample surface.

## V. RESULTS

The data presented below demonstrate that high-frequency NEMS actuation is quite easily accessible at room temperature, moderate vacuum (about 1 Torr) and magnetic fields small enough (under 0.9 T) to be achieved using a permanent magnet. By plotting the detected electrical signal vs. driving frequency, peaks at the mechanical resonance of the beam are observed. A typical result, showing two peaks, corresponding to each of the two resonator beams in this device pair, is plotted in Figure 4. A more detailed study of the right hand side peak at different driving amplitudes is shown in Figure 5, where the electronic background is subtracted from these data. After this de-embedding process, the resonance is fitted to a Lorentzian shape, from which a quality factor of 2800 can be inferred. Driving the beam with a voltage greater than  $3\mu\text{V}$  results in nonlinear behavior. At this drive power, the signal-to-noise ratio is approximately 20. As was discussed above, the signal strength varies as  $B^2$ . Therefore, a reduction in magnetic field from 900 mT to 300 mT, a level that is easily achieved with cm-scale permanent magnets, should still produce a peak with a signal-noise level of above 2.

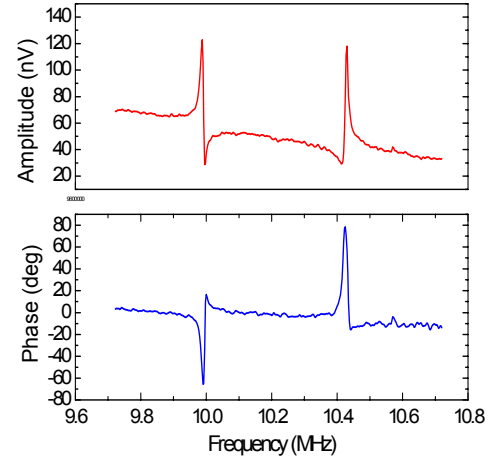


Figure 4. Measurement of mechanical resonance by magnetomotive transduction, performed at room temperature under 600 mTorr pressure. A magnet field of 0.9 Tesla provided by a NdFeB permanent magnet is used for these measurements.

The analysis of the resonant behavior of the beam is complicated by two factors. First, the beam is composed of two layers: 30 nm of Al and 30 nm of 3C-SiC. Second, both the suspended 3C-SiC layer and the Al layer are under stress as deposited; the SiC stress is tensile, while the Al stress is compressive. By solving the equation of motion, the resonant frequency  $f_0$  of a rectangular doubly clamped beam under zero tension is given by

$$f_0 = 1.03 \frac{w}{L^2} \sqrt{\frac{E_e}{\rho_e}} \quad (3)$$

where  $w$  is the beam width in the plane of vibration,  $L$  is the length,  $E_e$  is the effective Young's modulus, and  $\rho_e$  is the effective density of composite beam. For a composite beam, these parameters are given by

$$E_e = \frac{E_{\text{SiC}} A_{\text{SiC}} + E_{\text{Al}} A_{\text{Al}}}{A_{\text{SiC}} + A_{\text{Al}}} \quad (4)$$

$$\rho_e = \frac{\rho_{\text{SiC}} A_{\text{SiC}} + \rho_{\text{Al}} A_{\text{Al}}}{A_{\text{SiC}} + A_{\text{Al}}} \quad (5)$$

where  $A_{\text{SiC}}$  and  $A_{\text{Al}}$  are the area of Al and SiC. For the beam under study, Eq. 3 predicts a zero-stress resonant frequency  $f_0$  of 6.43 MHz. The aluminum layer causes a 36% reduction in  $E/\rho$  relative to a pure SiC beam, and therefore the resonant frequency of a pure SiC beam would be 20% higher than the composite beam.

Both the SiC and aluminum layers are under axial stress. For a rectangular beam under axial stress, the resonant frequency is given by [16]

$$f_\sigma = f_0 \sqrt{1 + \frac{\sigma L^2}{3.4 E_e w^2}} \quad (6)$$

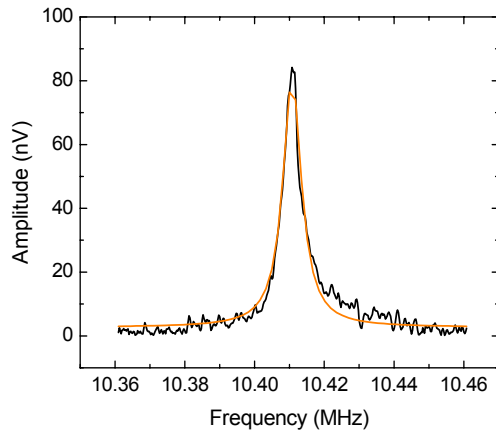


Figure 5. The drive is then reduced to  $3\mu\text{V}$  to ensure the linearity of the response. The plot shows de-embedded resonance peak. A Lorentzian fit indicates the quality factor of the resonance is about 2800.

where  $\sigma$  is the stress. Using Eq. (6) together with Eq. (3), we can extract the average stress in the beam. For the beam in this study, this comes to 79 MPa. This value reflects a weighted average of the stresses in the two layers, with the stiffness of the layer as the weighting factor. Because of the much higher stiffness of the SiC layer, the tensile stress dominates. Varying the thickness of the aluminum layer should provide a way to tune the frequency of SiC NEMS beams, by changing both the beam stiffness and residual stress.

## VI. CONCLUSION

SiC nanomechanical resonators were fabricated using electron beam lithography and reactive ion etching. NEMS beams consisting of 30 nm-thick 3C-SiC and 30 nm Al, with a width of 100 nm and a length of 12  $\mu\text{m}$ , show resonance at  $\sim 10\text{MHz}$ . Readout of this resonance is possible at room temperature, in moderate vacuum, and at relatively low magnetic fields. Progress toward compact and facile readout of NEMS devices is crucial toward practical applications of this technology.

## ACKNOWLEDGMENT

This work was partially supported by the Nanoscale Science and Engineering Initiative of the National Science Foundation under NSF Award Number CHE-0117752 and by the New York State Office of Science, Technology, and Academic Research (NYSTAR).

## REFERENCES

- [1] Roukes M L, *Sci. Am.* 285,2001, 48.
- [2] Roukes M L, *Phys. World* 14,2001, 25.
- [3] Craighead H G, *Science* 290, 2000, 1532.

- [4] Nguyen C T C, Katehi L P B and Rebeiz G M, *Proc. IEEE* 86 1998, pp. 1756.
- [5] Huang, X. M. H., Zorman, C. A., Mehregany, M. & Roukes, M. L. Nanodevice motion at microwave frequencies. *Nature* 421, 2003, pp. 496-496.
- [6] Ekinci, K. L., Huang, X. M. H. & Roukes, M. L. "Ultrasensitive nanoelectromechanical mass detection", *Appl. Phys. Lett.* 84, 2004, pp. 4469-4471.
- [7] Harrington, D. A. Ph.D. Thesis, Caltech, unpublished.
- [8] Huang, X.M.H. Ph.D. Thesis, 2004, Caltech.
- [9] Zorman, C. A. et al, "Epitaxial-growth of 3C-SiC films on 4 inch diam (100)silicon- wafers by atmospheric-pressure chemical-vapor-deposition", *J. Appl. Phys.* 78, 1995, pp. 5136-5138.
- [10] S. Timoshenko, D. Young, and W. Weaver, "Vibration problems in engineering, Wiley, New York, 1974
- [11] Cleland A N and Roukes M L, *Appl. Phys. Lett.* 1996, pp. 69 2653
- [12] Cleland A N and Roukes M L 1999 *Sens. Actuator A-Phys.*, 1999, 72 256
- [13] Cleland, A. N. & Roukes, M. L. A nanometre-scale mechanical electrometer. *Nature* 392, 1998, pp. 160-162.
- [14] Huang, X.M.H. Manolidis, M., Seong Chan Jun, & Hone, J. "Nanomechanical hydrogen sensing", *Appl. Phys. Lett.* 86, 2005, 143104.
- [15] Ekinci, K. L., Yang, Y. T., Huang, X. M. H. & Roukes, M. L. Balanced electronic detection of displacement in nanoelectromechanical systems. *Appl. Phys. Lett.* 81, 2002, pp. 2253-2255.
- [16] Bokaian, A., *Journal of Sound and Vibration*, 142, 1990, pp. 481